Aerodynamic Modelling of Unmanned Aerial System through Nonlinear Vortex Lattice Method, Computational Fluid Dynamics and Experimental Validation - Application to the UAS-S45 Bàlaam: Part 1.

Maxime Alex Junior KUITCHE[1], Ruxandra Mihaela BOTEZ*,[1], Arthur GUILLEMIN[1], David COMMUNIER[1]

*Corresponding author
[1]ETS, Laboratory of Active Controls, Avionics and AeroServoElasticity LARCASE, 1100 Notre Dame West, Montreal, Que., Canada, H3C-1K3, maxime-alex-junior.kuitche.1@ens.etsmtl.ca, ruxandra.botez@etsmtl.ca*, arthur.guillemin.ag@gmail.com, david.communier.1@ens.etsmtl.ca

DOI: 10.13111/2066-8201.2020.12.1.9

Received: 22 December 2019/ Accepted: 23 January 2020/ Published: March 2020

Abstract: *This paper describes a methodology to predict the aerodynamic behaviour of an Unmanned Aerial System. Aircraft design and flight dynamics modelling are mainly concerned with aerodynamics, and thus its estimation requires a high level of accuracy. The work presented here shows a new non-linear formulation of the classical Vortex Lattice Method and a comparison between this methodology and an experimental analysis. The new non-linear Vortex Lattice Method was performed by calculating the viscous forces from the strip theory, and the forces generated by the vortex rings from the vortex lifting law. The experimental analysis was performed on a reduced scale wing in a low speed wind tunnel. The obtained results were also compared to those obtained from semi-empirical methods programmed using DATCOM and our Fderivatives new in-house codes. The results have indicated the accuracy of the new formulation and showed that an aerodynamic model obtained with the aerodynamic coefficients predicted with this method could be useful for flight dynamics estimation.*

Key Words: *Aerodynamic modelling, Experimental analysis, Vortex Lattice Method, UAS-S45, Wind Tunnel Tests*

1. INTRODUCTION

The focus of flight dynamics modelling is mostly related to its ability to accurately predict a suitable aerodynamic model. During the first half of the 20th century, wind tunnel testing was the core of aerodynamic research and it was the best way to obtain an accurate aerodynamic model of an aircraft [1]. Aerodynamic semi-empirical analyses were performed using charts and equations from wind tunnel and flight tests, such as those presented in the USAF DATCOM procedure [2]. Since 1960s, due to the advancement in computer capabilities, numerical methodologies quickly gained ground such as Vortex Lattice Method (VLM). The VLM estimates the aerodynamic model of a lifting surface, such as wing, using an infinite number of horseshoe vortex. Many researchers used alternative and corrected formulation of the Vortex Lattice Method. Chaparo et *al.* [3] used a corrected three-dimensional VLM to

estimate transonic aerodynamic loading and wave drag for a transport aircraft. Dos santos and Marques [4] coupled the Vortex Lattice Method with a Kirchhoff flow to predict the lift stall. Murua et *al*. used an unsteady formulation of the VLM to estimate aeroelasticity and to perform a flight dynamic simulation.

In this paper, a new nonlinear formulation of the Vortex Lattice Method is presented. The new non-linear Vortex Lattice Method was performed by calculating the viscous forces from the strip theory, and the forces generated by the vortex rings from the vortex lifting law. This methodology showed its efficacity in accurately calculating the effects of viscosity using low computational resources.

The estimation presented in this paper was carried out with the aim to design an UAS-S45 flight simulator. The aerodynamic coefficients obtained using the new non-linear VLM, and the CFD method were compared to those obtained using the in-house developed Fderivatives code [5–7] at the LARCASE.

This code is based on improvements of the DATCOM procedure aerodynamic formulations and was developed in-house at our Research Laboratory in Active Controls, Avionics and Aeroservoelasticity (LARCASE) of the ETS. Fderivatives code can accurately estimate the aircraft aerodynamic coefficients and their corresponding stability derivatives' from a minimum amount of geometrical data.

Based on the results of the investigation of the flow around aircraft [8, 9], and by highlighting the necessity of an experimental validation, the numerical procedures thereby established was compared to experimental wind tunnel test results for a reduced scaled UAS-S45 wing.

The non-linear VLM is detailed in Section 2. The experimental procedure is presented in Section 3 and the Fderivatives methodology in Section 4. The results are presented in Section 5 and are followed by the Conclusions.

2. NEW NON-LINEAR VORTEX LATTICE METHOD

The classical VLM is based on the resolution of the Laplace Eq. (1) for a potential flow by assuming a boundary condition of zero flow in the normal direction to the wing surface.

$$\nabla\left(\boldsymbol{V}_p + \varphi\right).\boldsymbol{n} = 0 \tag{1}$$

where, $\boldsymbol{V}_\infty$ is the free-stream flow, φ is the perturbation potential, and $\boldsymbol{n}$ is the vector normal to the wing surface.

In order to compute the aerodynamic forces and moments by using the classical VLM, the wing is initially divided into panels. A vortex ring is placed on the quarter chord of each panel, and a collocation point is placed at 75% of the quarter chord line from the leading edge. The velocity induced by each vortex ring to an arbitrary point is given by the Biot-Savart law:

$$\boldsymbol{V} = \frac{\Gamma}{4\pi}\frac{\boldsymbol{r}_1 \times \boldsymbol{r}_2}{\left|\boldsymbol{r}_1 \times \boldsymbol{r}_2\right|^2}\boldsymbol{r}_0 \cdot \left(\frac{\boldsymbol{r}_1}{\boldsymbol{r}_2} - \frac{\boldsymbol{r}_2}{\boldsymbol{r}_1}\right) \tag{2}$$

where Γ is the vortex intensity, $\boldsymbol{r_1}$ is the position vector from the beginning of the vortex line to an arbitrary point, $\boldsymbol{r_2}$ is the position vector from the end of the vortex line to an arbitrary point, and $\boldsymbol{V}$ is the induced velocity.

The unknown velocities of the vortex rings are determined by considering that the Eq.(1) is satisfied, which leads to the following equation:

$$\left(\boldsymbol{V}_{\infty} + \sum_{j=1}^{N} \Gamma_j \boldsymbol{v}_{ij} \right) . \boldsymbol{n}_i = 0 \tag{3}$$

where $\boldsymbol{V}_{\infty}$ is the freestream velocity, N is the total number of the vortex ring, $\boldsymbol{n_i}$ is the surface normal vector computed at the ith collocation point, $\boldsymbol{V_{ij}}$ is the velocity induced by the j^{th} vortex ring at the i^{th} collocation point.

In the new nonlinear VLM [10], the vortex rings intensities are adjusted by using nonlinear viscous data. A correction parameter is thus added to the vortex intensities. The corrected vortex rings intensities are given by:

$$\Gamma_j + \Delta\Gamma_j \tag{4}$$

The addition of a correction on the vortex rings intensities leads to obtaining a second induced velocity field, which converts Eq. (3) into following Eq. (5):

$$\left(\boldsymbol{V}_{\infty} + \sum_{j=1}^{N} \left(\Gamma_j + \Delta\Gamma_j \right) \boldsymbol{v}_{ij} + \boldsymbol{V}_i^T \right) . \boldsymbol{n}_i = 0 \tag{5}$$

where $\boldsymbol{V}^{\mathrm{T}}_{\mathrm{i}}$ is the surface transpiration velocity. For simplification, it is assumed that:

$$\boldsymbol{V}_i^T = \boldsymbol{V}_i^T . \boldsymbol{n}_i \tag{6}$$

The following Eq. (7) is obtained by combining Eqs. (3), (5), and (6):

$$\sum_{j=1}^{N} \boldsymbol{v}_{ij} . \boldsymbol{n}_i \Delta\Gamma_j = -\boldsymbol{V}_i^T \tag{7}$$

A strip analysis of the wing is performed to obtain an additional set of equations needed for the problem resolution [10]. This strip analysis was used to calculate a set of nonlinear viscous pressure coefficient distribution. For this purpose, the wing was divided into span-wise panels, on which a control point was defined. The nonlinear viscous pressure coefficient distribution was thus calculated for local flow, for each span-wise strip at its control point by using the two-dimensional viscous flow solver XFoil [11].

$$C_{p,i}^{visc} = f(\text{airfoil}_i, Re_i, \|\boldsymbol{V}_i\|, \alpha_i) \tag{8}$$

In Eq. (8), Re_{i} is the Reynolds number, and $\boldsymbol{V}_i$ is the total velocity at the control point given by:

$$\boldsymbol{V}_i = \boldsymbol{V}_{\infty} + \sum_{j=1}^{N} \left(\Gamma_j + \Delta\Gamma_j \right) \boldsymbol{v}_{ij} \tag{9}$$

where, $\boldsymbol{V}_{\infty}$ is the free-stream velocity, N is the total number of vortex rings over the wing, $\boldsymbol{v}_{\mathrm{ij}}$ is the velocity induced by the unit strength vortex ring j at the i^{th} strip control point, and α_i is the local effective angle of attack of the strip given by:

$$\alpha_i = \tan^{-1} \left[\frac{\left(\boldsymbol{V}_{\infty} + \sum_{j=1}^{N} \left(\Gamma_j + \Delta\Gamma_j \right) \boldsymbol{v}_{ij} \right) . \boldsymbol{n}_{s,i}}{\left(\boldsymbol{V}_{\infty} + \sum_{j=1}^{N} \left(\Gamma_j + \Delta\Gamma_j \right) \boldsymbol{v}_{ij} \right) . \boldsymbol{c}_{s,\mathrm{i}}} \right] \tag{10}$$

In Eq. (10), $\boldsymbol{n}_{s,i}$ is a unit vector in direction normal to the chord of the i^{th} strip and $\boldsymbol{c}_{s,j}$ is a unit vector in direction of the chord of the i^{th} strip. In the case of a large sweep angle, the strip theory analysis is replaced by a sweep analysis [10], and the effective angle of attack is corrected using the iterative methodology defined in [12, 13].

The corrected vortex ring intensities are estimated by assuming that the nonlinear viscous pressure coefficient variation obtained from the strip analysis is equal to the pressure coefficient variation obtained from the vortex ring intensities for each panel on the wing surface. This assumption leads to the following expression:

$$-\boldsymbol{F}_i.\boldsymbol{n}_i + A_i Q_\infty \Delta C_{p,i}^{visc} = 0 \tag{11}$$

where $\boldsymbol{F}_i$ is the aerodynamic force generated by all the vortex lines on the panel, $\boldsymbol{n}_i$ is the surface normal vector, A_i is the panel area, Q_∞ is the dynamic pressure, and $C_{p,i}^{visc}$ is the nonlinear viscous pressure coefficient.

For an arbitrary panel, the projected force $\boldsymbol{F_i}$ onto the direction of the local normal is derived from Eq. (11) using the three-dimensional vortex lifting law (12):

$$\begin{aligned} -\boldsymbol{F}_i.\boldsymbol{n}_i = \rho\left[\boldsymbol{n}_i \times \left(V_\infty + \sum_{j=1}^{N}\left(\Gamma_j + \Delta\Gamma_j\right)\boldsymbol{v}_{ij}\right)\right].\big[&\left(\Gamma_i - \Gamma_U\right)\gamma_{12} + \left(\Gamma_i - \Gamma_R\right)\gamma_{23} + \left(\Gamma_i - \Gamma_L\right)\gamma_{61} \\ &+ \left(\Gamma_U - \Gamma_{UR}\right)\gamma_{34} + \left(\Gamma_U - \Gamma_{UL}\right)\gamma_{56} + \left(\Delta\Gamma_i - \Delta\Gamma_U\right)\gamma_{12} + \left(\Delta\Gamma_i - \Delta\Gamma_R\right)\gamma_{23} \\ &+ \left(\Delta\Gamma_i - \Delta\Gamma_L\right)\gamma_{61} + \left(\Delta\Gamma_U - \Delta\Gamma_{UR}\right)\gamma_{34} + \left(\Delta\Gamma_U - \Delta\Gamma_{UL}\right)\gamma_{56} \end{aligned} \tag{12}$$

where ρ is the air density, γ is the geometrical segment of the vortex segment, the subscript U denotes the direct upstream ring, R and L are the right and left rings, and UR and UL are the upstream-right and upstream left rings, and the subscripts i indicates the current vortex rings.

By introducing Eq. (12) into Eq. (11) and coupling the result with Eq. (7), a system of $2N$ equations is obtained:

$$\boldsymbol{R} = \begin{Bmatrix} \vdots \\ -\boldsymbol{F}_i.\boldsymbol{n}_i + \boldsymbol{A}_i Q_\infty \Delta C_{p,i}^{visc} \\ \vdots \\ - - - - - - - - - \\ \vdots \\ \sum_{j=1}^{N} \boldsymbol{v}_{ij}.\boldsymbol{n}_i \Delta\Gamma_j + \boldsymbol{V}_i^T \\ \vdots \end{Bmatrix} = \boldsymbol{0} \tag{13}$$

This system of equations allowed calculating the N values of the intensities corrections and of the surface transpiration velocities needed to estimate the aerodynamic forces and moments.

3. EXPERIMENTAL ANALYSIS

A wind tunnel experiment was used to validate our computational fluid dynamics methodology. This experiment was performed in the Price-Paidousis low speed wind tunnel [14, 15]. This wind tunnel is composed of a power unit, a settling unit, a contraction unit and a test unit (Fig. 1).

The power unit is a room of 800 m² containing a 40hp power direct current motor driving a centrifugal fan. The fluid flow is parallel to the axis of rotation at the inlet of the air intakes, and is perpendicular to the axis of rotation at the outlet of the fan [14].

The settling unit directs the pressurized air from the power unit to the test chamber while giving it the desired flow characteristics. The settling unit contains a wide-angle diffuser that slows the fluid as much as possible on a short distance to maximize pressure retention. The resulting flow can then be changed and may become turbulent. Five rectifier filters have been re-added to the settling unit to improve the quality of the flow: 1 honeycomb filter to reduce eddies and 4 nylon filters with square pattern holes to produce the desired flow [14].

The contraction unit is a convergent base of 62.5×91.5 cm² downstream and of 200×200cm² upstream. It is designed to accelerate the fluid in order to reach its maximum speed.

The test unit or test chamber has a length of 182.5 cm, a height of 91.5cm and a width of 62.5 cm. Its size allows reduced scale models of wings to be tested when they are placed in its center.

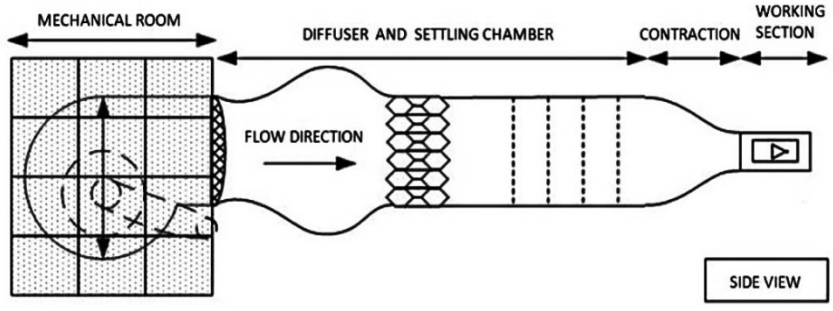

Fig. 1 Price-Paidousis wind tunnel sections

A wind tunnel calibration was made to determine the air flow conditions in the test chamber using the Log-Tchebycheff (Log-T) method (Fig. 2). The accuracy of the estimated local velocities using the Log-T method is often decreased due to Pitot tube measurements uncertainties. Mosbah et al. [16] developed a methodology to cope this decrease in accuracy. Their methodology used a minimum of dynamic pressure measurements from a Pitot tube, and estimated the dynamic pressure from a neural network that has been optimized with a great deluge algorithm. This methodology was applied in this work. The calibration of the wind tunnel was made using two airspeeds of: 5.5m/s and 26.5m/s.

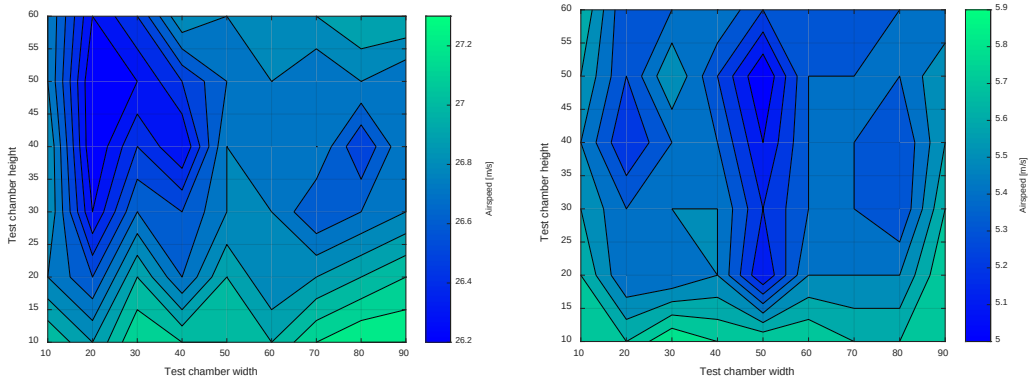

Fig. 2 Airflows obtained from the Log-Tchebycheff method

Figure 2 shows that the flow seems to be uniform in the test chamber. There is a contraction phenomenon at the border of the chamber which causes an acceleration of the fluid. Therefore, the wing model should be small enough to not be in contact with the flow on the border of the test chamber, and big enough to make possible the aerodynamic coefficient measurements.

The wind tunnel wing model was chosen to be a rectangular wing with a chord of 10 inches and a span of 12 inches, which corresponds to 2% of the surface of the test chamber. The wing model was built of wood. Five plywood ribs were cut and assembled using a spar, and the assembly was covered with thin strips of balsa wood. Very small amounts of plastic were then placed to smooth the surfaces and to make them uniform (Fig. 3).

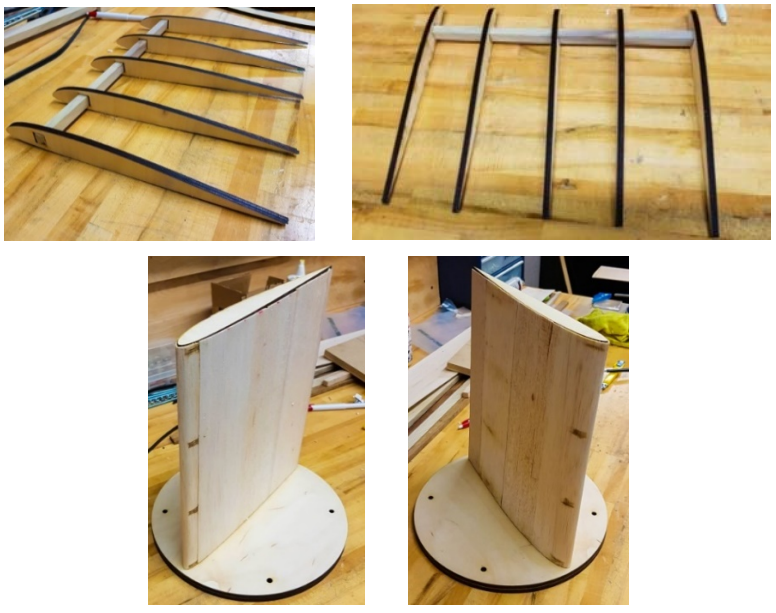

Fig. 3 UAS-S45 wing model setup

The wind tunnel tests were performed using an aerodynamic scale and a Pitot tube. The scale consists of two plates fixed on a force sensor, one being fixed to the test chamber, the other one being mounted on a gear assembly driven by a servomotor. This servomotor allows the angle of attack to be changed automatically during the test. A mini 40E sensor is connected to a National Instrument acquisition box. The data collected by the box can be directly read and stored with an interface realized using Labview software [15]. The Pitot tube is connected to an FKS 1DP-PBM meter for air pressure, speed and flow measurements (Fig. 4). The FKS 1DP-PBM is used to obtain the airflow velocity inside the test chamber knowing the temperature, the humidity, the *K*-factor and the ambient pressure.

a) b) c)

Fig. 4 Pitot tube (a); FKS 1DP-PBM meter (b); mini 40E (c)

4. FDERIVATIVES' METHODOLOGY

While experimental analysis gives accurate results on aerodynamic estimations, they can be very demanding in terms of time and budget. Semi-empirical methods such as our in-house Fderivatives are often used to avoid those drawbacks.

Fderivatives is a collection of methodologies and algorithms for estimating aircraft aerodynamic coefficients and stability derivatives. Primarily designed as an improvement of the classical DATCOM procedure [2], its main improvements are related to the calculation of the aerodynamics characteristics for airfoils, and for entire aircraft in the "Wing-Body-tail" configuration. The accuracy of an airfoil's aerodynamic parameters' estimation has a major influence on the aerodynamics results for that aircraft. To validate an airfoil's aerodynamic parameters, Popescu [17] performed numerical calculations using DATCOM and Fderivatives codes on NACA 4, 5, 6 and 6A digits airfoils. For a collection of 30 airfoils, the estimated the lift curve slope, the zero-lift angle of attack and the maximum lift coefficient for a range of Mach numbers from 0.1 to 0.3, and Reynolds numbers from 1×10e6 to 9×10e6. The results gave mean errors of 1.91%, 3.52% and 6.85% between the experimental and the estimated values of the lift curve slope, the zero-lift angle of attack and the maximum lift coefficient, respectively. In the same way, Anton et al. [5] validated the results obtained for an aircraft in a "Wing-Body-tail" configuration. The estimations were performed on a X-31 aircraft. The lift, drag and pitch moment coefficients obtained experimentally in a wind tunnel were compared to those obtained using Fderivatives, DATCOM and the Jorgensen methods. The calculations were performed for a Mach number of 0.18, a Reynolds number of 2.07×10e7 based on the mean aerodynamic chord, and a range of angles of attack from -2° to 20°. The results have shown a decrease in the estimation errors of 11% by using Fderivatives compared to two other methods (DATCOM and Jorgensen) errors.

The Fderivatives code was used in this paper to estimate the aerodynamic behaviour of the UAS-S45 airfoil, and entire geometry in "Wing-Body-Tail" configuration (Fig. 5). Compared to other methods, the Fderivatives code used a minimum amount of geometrical data to obtain its results. The wing was represented using its airfoil coordinates at the tip, the MAC and the root position, as well as its aspect and taper ratios, its area, its dihedral and its quarter chord sweep angles. The horizontal and the vertical tail were defined in the same way as the wing. The fuselage was analysed as divided in 20 elliptical cross sections along the length of the UAS-S45. The nose, the forebody and the afterbody of the UAS were assumed to have conical shapes. The Fderivatives code does not take into account the geometries of the winglets, the landing gear or the twin vertical tail. Therefore, the winglets and the landing gear were neglected, and the twin vertical tail was replaced by a single vertical tail having twice the area of each of the original tails.

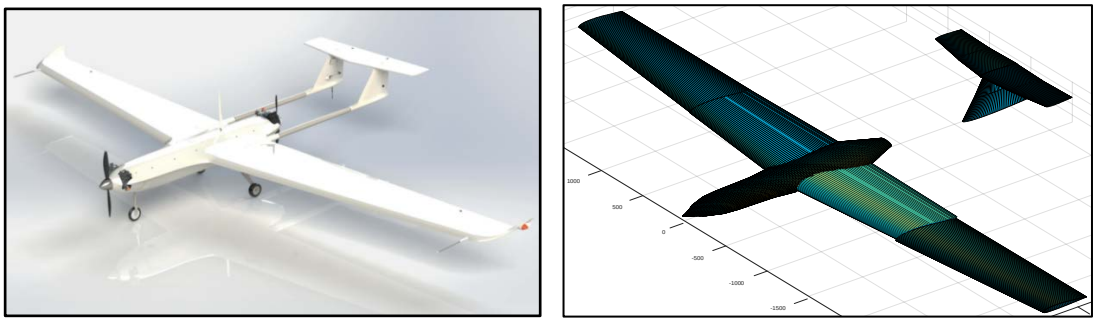

Fig. 5 UAS-S45 in "Wing-Body-Tail" configuration in Fderivatives

5. RESULTS AND DISCUSSIONS

In this chapter, the relative error is defined as being calculated between a reference value x_a and an approximated value x_b with the equation $\left|\frac{x_b - x_a}{x_a}\right| * 100\%$.

5.1 Validation of the Numerical Procedure

In order to validate the numerical approach, the CFD and experimental analysis results on a reduced scale model of the UAS-S45 wing were compared. A polyhedral mesh grid was generated with 4,716,118 cells. Table 1 presents the characteristics of the mesh grid model.

Fig. 6 Mesh grid model of the UAS-S45 wing

Table 1. UAS-S45 wing model mesh parameters

Parameters	Number of cells	1st layer height	Number of layers in the inflation	Orthogonal quality average	Skewness average
values	4,716,118	0.002m	10	0.8166	0.37977

The simulation used a *k-ω* SST model as "turbulence model". In the wind tunnel test chamber, the flow on the walls was laminar. The wing model was fixed to the test unit floor, and the flow around the wing tip was "laminar". However, during the numerical simulation of a finite wing, the higher air pressure under the wing tried to move around the tip towards the lower pressure above the wing, and then creates trailing vortices. To cope with this problem in CFD analysis and to obtain the same flow as the one in the experiment analysis, a symmetry condition was added on the wing tip (Fig. 7).

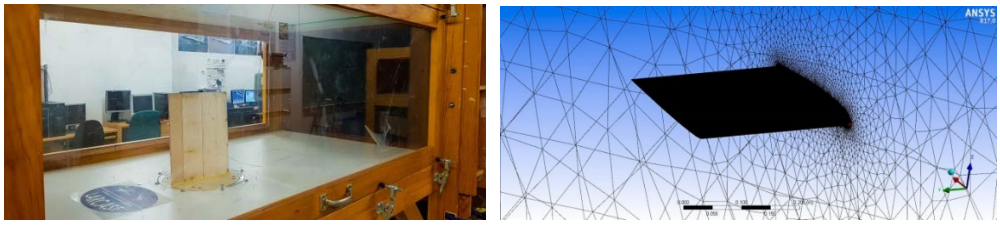

Fig. 7 UAS-S45 wing model symmetry condition

The experimental (Section 3) and the numerical analyses were performed for the following specific flow conditions: speeds V =10m/s, 20m/s, 30m/s; altitude alt = 0ft, and for a range of angles of attack between -10° and 10°. Figure 8 shows the lift coefficients obtained using numerical and experimental approaches as functions of speeds. It is obvious that the speed has no significant influence on the results. The non-influence of speed could be explained by the fact that the flow remains subsonic, and the Mach number M remains smaller than 0.2. Thus, the compressible effect of the flow is neglected.

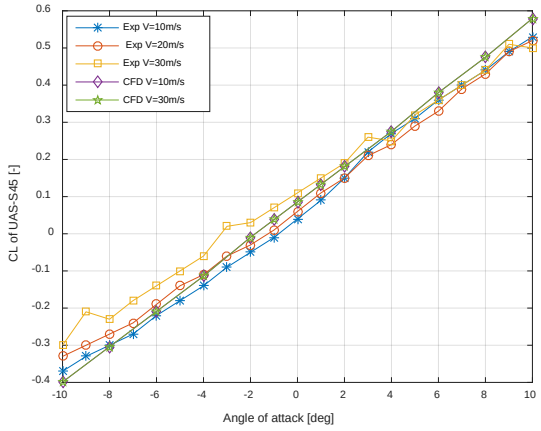

Fig. 8 Experimental and numerical lift coefficients' variations with angle of attack for several airspeeds

Next, the numerical and experimental lift and drag coefficients for varying angles of attack were compared. Figures 9 and 10 shows a test case for the speed v = 30m/s, and altitude alt = 0ft.

This test case was selected because this airspeed makes it possible to obtain a drag force much higher than the sensor noise, and thus to facilitate the measurements process. It has been noticed that there a very good agreement between the CFD ANSYS Fluent software, the nonlinear VLM and the experimental analysis results for both lift and drag coefficients variations (Fig. 9).

However, a small relative error was found between the lift variations with angle of attack) obtained using experimental testing, the numerical CFD and nonlinear VLM theories, as well as the DATCOM and Fderivatives' semi-empirical methodologies (Fig. 10).

These differences (relative errors) could be explained by the presence of the "trailing vortices" calculated using the finite wing theory. These trailing vortices were neglected for the case of the CFD analysis, and for the case of the nonlinear VLM these trailing vortices depend on the number of strips considered in the strip analysis. This comparison confirmed the superiority of the CFD theory, as well as of the proposed nonlinear VLM with respect to the other numerical approaches, along with its performance validation with respect to the experimental results values.

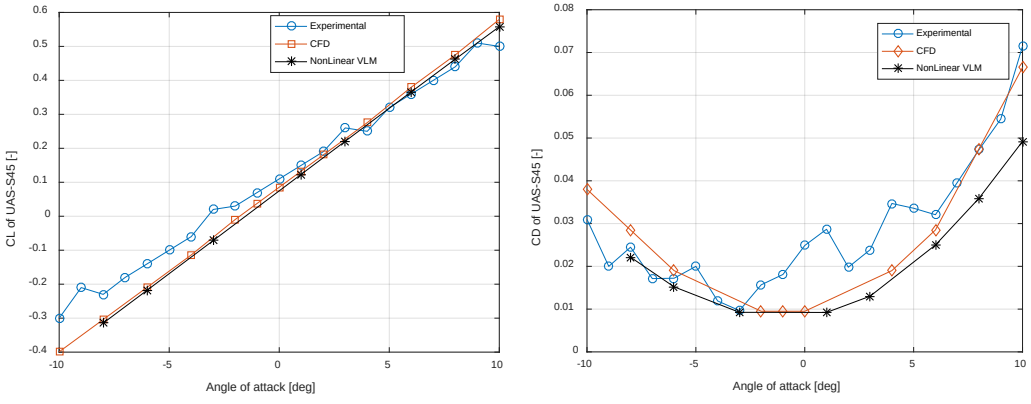

Fig. 9 Comparison between the lift and drag coefficients' variations with angles of attack obtained with experimental, nonlinear VLM and CFD analyses for V=30m/s

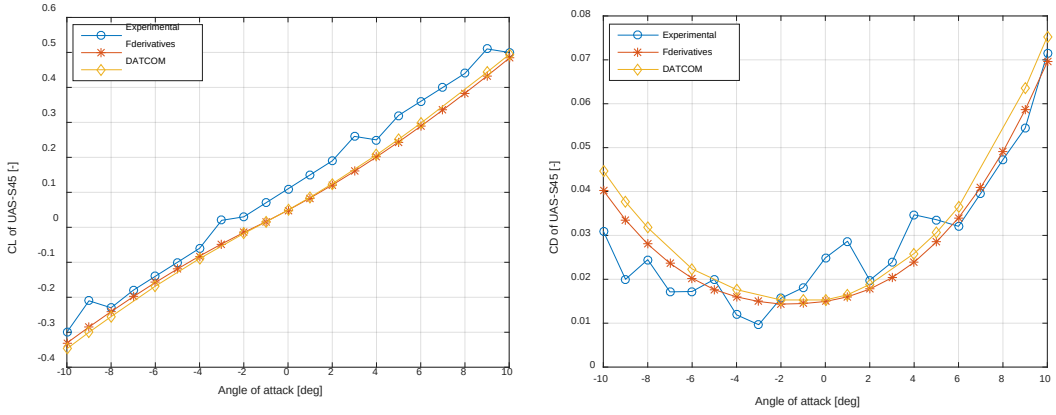

Fig. 10 Comparison between the lift and drag coefficients' variations with angles of attack obtained with experimental analysis, DATCOM and Fderivatives procedure for V= 30m/s

The CFD and the nonlinear VLM results were compared to the results obtained from Fderivatives and DATCOM semi-empirical codes. Since no significant variation of the aerodynamic coefficients with the Mach number and the altitude was found, the three numerical methodologies results were shown here only for one flight condition, expressed in terms of Mach number 0.14 and altitude of 10,000 ft (Fig. 11). The graphs shown in Fig. 11 clearly show that there is a close agreement for the lift coefficients variations calculated using all four methodologies. The drag coefficients variations, on the contrary, show a significant difference between values calculated with 3 methods, and values calculated with the CFD analysis, especially for high negative angle of attack values (-10° to -2°).

The CFD analysis predicts the stall at approximately -12°, and therefore the drag coefficient increases rapidly around this value. The nonlinear VLM, Fderivatives and DATCOM codes, however, predict the stall for angles of attack far above 12°, and thus the drag coefficients estimated from these three methodologies maintain do not increase fast.

As expected, the zero-lift drag and the zero-lift pitch moment coefficients variations have different values obtained with Fderivatives, DATCOM and CFD analyses codes (Fig. 11). These values differences are small, and are mainly influenced by the airfoil aerodynamics coefficient, are estimated using semi-empirical interpolations in DATCOM and Fderivatives codes. However, the nonlinear VLM predict with a good accuracy the zero-lift pitch because the airfoil aerodynamic coefficient is estimated using Xfoil.

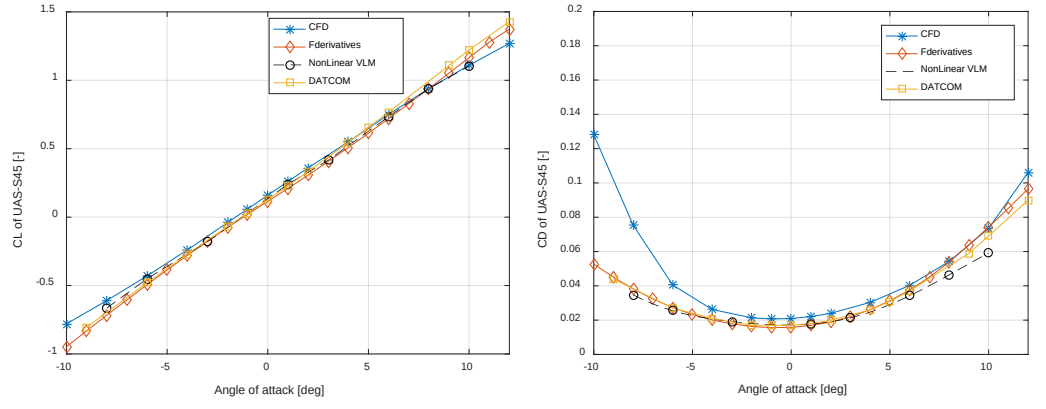

a) b)

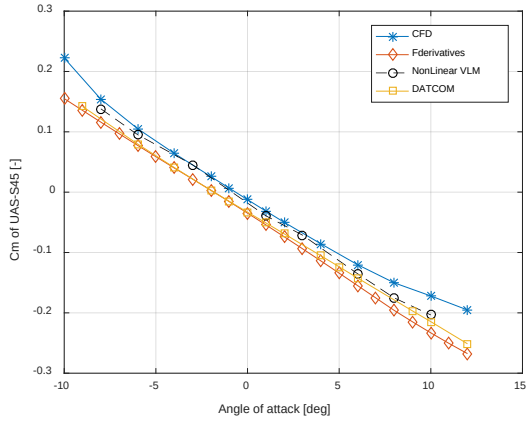

c)

Fig. 11 Comparison of the UAS-S45 lift (a), drag (b) and pitch moment (c) coefficients' variations with the angle of attack obtained using CFD, nonlinear VLM, Fderivatives and DATCOM theories for M = 0.14 and altitude H = 10,000ft

Figure 12 shows the longitudinal lift and moment derivatives values with respect to pitch rate, and for a range of angles of attack (-10° to 12°), C_{Lq} and C_{mq} , for the UAS-S45. The estimation was made for a Mach number of 0.14 and an altitude of 5,000ft. The CFD analysis, Fderivatives and DATCOM codes estimated constant lift and moment derivatives with respect to pitch rate C_{Lq} and C_{mq} as shown on Figure 12. There is a rather good agreement between the three methodologies results for the moment derivative with respect to pitch rate, C_{mq}, with a relative error 1.3%, and a similar observation on the lift derivative with respect to pitch rate, C_{Lq}, with a relative error of 4.7%.

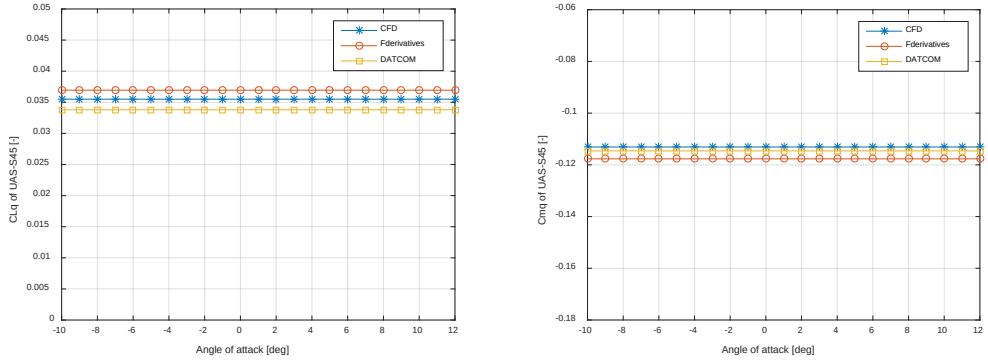

a) b)

Fig. 12 Comparison of the lift (a) and moment derivatives (b) with respect to pitch rate variation with the angle of attack of the UAS-S45 obtained using CFD, Fderivatives and DATCOM for M = 0.14 and altitude = 5,000 ft

6. CONCLUSIONS

This paper presents a methodology designed to predict the aerodynamic behaviour of the unmanned aerial system UAS-S45 of Hydra Technologies. A nonlinear Vortex Lattice Method was introduced. The method consisted in calculating the viscous forces from the strip theory, and the forces generated by the vortex rings from the vortex lifting law.

This methodology results were validated with experimental analysis results on a reduced scale model of the UAS-S45. An experimental simulation was made on a 12×10 in wing in the Price-Paidoussis wind tunnel. The lift and drag coefficients obtained were compared to those from a computational fluid dynamics analysis of the same wing. Finally, the results obtained from new nonlinear Vortex Lattice Method were compared to results from DATCOM and Fderivatives. This comparison reveals shows a good agreement of the different approaches and prove our results to be highly accurate.

ACKNOWLEDGEMENTS

Special thanks are due to the Natural Sciences and Engineering Research Council of Canada (NSERC) for the Canada Research Chair Tier 1 in Aircraft Modelling and Simulation Technologies funding. We would also like to thank Mrs. Odette Lacasse and Mr. Oscar Carranza for their support at the ETS, as well as to Hydra Technologies' team members Mr. Carlos Ruiz, Mr. Eduardo Yakin and Mr. Alvaro Gutierrez Prado in Mexico for their collaboration.

REFERENCES

[1] T. E. Nelson, D. W. Zingg, Fifty Years of Aerodynamics: Successes, Challenges, and Opportunities, *Canadian Aeronautics and Space Journal*, **50**, 61–84, doi:10.5589/q04-003, 2004.

[2] J. E. Williams, S. R. Vukelich, *The USAF Stability and Control Digital DATCOM*, Volume **I**, Users Manual. McDonnell Douglas Astronautics Company, Air Force Flight Dynamics Laboratory, 1979.

[3] D. Chaparro, G. E. Fujiwara, E. Ting, N. T. Nguyen, *Aerodynamic Modeling of Transonic Aircraft Using Vortex Lattice Coupled with Transonic Small Disturbance for Conceptual Design*, In: 34th AIAA Applied Aerodynamics Conference, American Institute of Aeronautics and Astronautics, Washington, D.C., 2016.

[4] C. R. dos Santos, F. D. Marques, Lift Prediction Including Stall, Using Vortex Lattice Method with Kirchhoff-Based Correction, *Journal of Aircraft*, doi:10.2514/1.C034451, 2017.

[5] N. Anton, R. M. Botez, D. Popescu, Stability Derivatives for a Delta-Wing X-31 Aircraft Validated using Wind Tunnel Test Data, *Proceedings of the Institution of Mechanical Engineers, Part G: Journal of Aerospace Engineering*, **225**, 403–416, doi:10.1243/09544100JAERO799,2011.

[6] N. Anton, R. Botez, D. Popescu, *New Methodologies for Aircraft Stability Derivatives Determination from Its Geometrical Data*, In: AIAA Atmospheric Flight Mechanics Conference. p. 6046. American Institute of Aeronautics and Astronautics, Chicago, Illinois, 2009.

[7] N. Anton, R. M. Botez, D. Popescu, New Methodology and Code for Hawker 800XP Aircraft Stability Derivatives Calculation from Geometrical Data, *The Aeronautical Journal*, **114**, 367–376, doi:10.1017/S0001924000003821, 2010.

[8] O. J. Boelens, CFD Analysis of the Flow Around the X-31 Aircraft at High Angle of Attack, *Aerospace Science and Technology*, **20**, 38–51, doi:10.1016/j.ast.2012.03.003, 2012.

[9] A. Schütte, O. J. Boelens, M. Oehlke, A. Jirásek, T. Loeser, Prediction of the Flow Around the X-31 Aircraft Using Three Different CFD Methods, *Aerospace Science and Technology*, **20**, 21–37, doi:10.1016/j.ast.2011.07.014, 2012.

[10] O. Şugar Gabor, A. Koreanschi, R. M. Botez, A New Non-Linear Vortex Lattice Method: Applications to Wing Aerodynamic Optimizations, *Chinese Journal of Aeronautics*, **29**, 1178–1195, doi:10.1016/j.cja.2016.08.001, 2016.

[11] M. Drela, *XFOIL: An Analysis and Design System for Low Reynolds Number Airfoils*, In: Low Reynolds Number Aerodynamics, pp. 1–12, Springer, Berlin, Heidelberg, 1989.

[12] A. Elham, Adjoint Quasi-Three-Dimensional Aerodynamic Solver for Multi-Fidelity Wing Aerodynamic Shape Optimization, *Aerospace Science and Technology*, **41**, 241–249, doi:10.1016/j.ast.2014.12.024, 2015.

[13] J. Mariens, A. Elham, M. J. L. van Tooren, Quasi-Three-Dimensional Aerodynamic Solver for Multidisciplinary Design Optimization of Lifting Surfaces, *Journal of Aircraft*, **51**, 547–558, doi:10.2514/1.C032261, 2014.

[14] M. Flores Salinas, *Méthodologies Nouvelles pour la Réalisation d'Essais dans la Soufflerie Price-Païdoussis*, http://espace.etsmtl.ca/1565/, 2015.

[15] D. Communier, M. F. Salinas, O. Carranza Moyao, R. M. Botez, *Aero Structural Modeling of a Wing using CATIA V5 and XFLR5 Software and Experimental Validation using the Price- Païdoussis Wing Tunnel*, In: AIAA Atmospheric Flight Mechanics Conference. p. 2558. American Institute of Aeronautics and Astronautics, Dallas, Texas, 2015.

[16] A. Ben Mosbah, M. Flores Salinas, R. Botez, T. Dao, New Methodology for Wind Tunnel Calibration Using Neural Networks - EGD Approach, *SAE International Journal of Aerospace*, **6**, 761–766, doi:10.4271/2013-01-2285, 2013.

[17] D. Popescu, *Nouvelle Implémentation de la Procédure DATCOM pour le Calcul des Coefficients Aérodynamiques et des Dérivées de Stabilité dans le Domaine Subsonique de Vol*, http://espace.etsmtl.ca/74/, 2009.